Tuning the magnetocrystalline anisotropy of Fe₃Sn by alloying

Olga Yu. Vekilova[*]

Department of Physics and Astronomy, Uppsala University, Box 516, 75121 Uppsala, Sweden

Bahar Fayyazi, Konstantin P. Skokov, and Oliver Gutfleisch

Materials Science, TU Darmstadt, Alarich-Weiss-Str. 16, 64287 Darmstadt, Germany

Cristina Echevarria-Bonet and José Manuel Barandiarán

BCMaterials, UPV/EHU Science Park, 48940 Leioa, Spain

Alexander Kovacs, Johann Fischbacher, and Thomas Schrefl

Department for Integrated Sensor Systems, Danube University Krems, Viktor Kaplan Str. 2/E, 2700 Wiener Neustadt, Austria

Olle Eriksson

Department of Physics and Astronomy, Uppsala University, Box 516, 75121 Uppsala, Sweden
and School of Science and Technology, Örebro University, SE-701 82 Örebro, Sweden

Heike C. Herper

Department of Physics and Astronomy, Uppsala University, Box 516, 75121 Uppsala, Sweden

The electronic structure, magnetic properties, and phase formation of hexagonal ferromagnetic Fe₃Sn-based alloys have been studied from first principles and by experiment. The pristine Fe₃Sn compound is known to fulfill all the requirements for a good permanent magnet, except for the magnetocrystalline anisotropy energy (MAE). The latter is large, but planar, i.e., the easy magnetization axis is not along the hexagonal c direction, whereas a good permanent magnet requires the MAE to be uniaxial. Here we consider Fe₃Sn₀.₇₅M₀.₂₅, where $M =$ Si, P, Ga, Ge, As, Se, In, Sb, Te, Pb, and Bi, and show how different dopants affect the MAE and can alter it from planar to uniaxial. The stability of the doped Fe₃Sn phases is elucidated theoretically via the calculations of their formation enthalpies. A micromagnetic model is developed to estimate the energy density product $(BH)_{max}$ and coercive field $\mu_0 H_c$ of a potential magnet made of Fe₃Sn₀.₇₅Sb₀.₂₅, the most promising candidate from theoretical studies. The phase stability and magnetic properties of the Fe₃Sn compound doped with Sb and Mn have been checked experimentally on the samples synthesised using the reactive crucible melting technique as well as by solid state reaction. The Fe₃Sn-Sb compound is found to be stable when alloyed with Mn. It is shown that even small structural changes, such as a change of the c/a ratio or volume, that can be induced by, e.g., alloying with Mn, can influence anisotropy and reverse it from planar to uniaxial and back.

I. INTRODUCTION

Strong permanent magnets creating high magnetic fields are of ultimate importance for many technological applications, from magnetic resonance imaging to magnetic hard disk drives in information storage. They are also used in a number of green energy applications, like motors for hybrid and electric cars and direct-drive wind turbines [1]. The strongest known permanent magnets typically contain rare earth elements [2]. For the past few decades, the demand for such magnets has substantially increased. As the cost of the rare-earth-based materials is high, the search for magnets that are cheaper and contain smaller amounts of rare earth elements has become an important field of research [1,3,4].

Ferromagnets with rather high Curie temperature (T$_C$) above 400 K and high saturation magnetization as well as high magnetocrystalline anisotropy energy (MAE) are considered as good candidates for permanent magnet applications. Furthermore, for such materials the axis corresponding to the longest lattice constant, i.e., the c axis in most hexagonal structures should be the unique easy magnetization direction [1,3,4]. These properties can be found, in particular, in Fe-rich materials with noncubic uniaxial crystal structures. The hexagonal Fe₃Sn compound satisfies these conditions to a large degree. Among five existing intermetallic compounds containing Fe and Sn, the Fe₃Sn phase is one of the most attractive ones, due to the highest concentration of iron and therefore highest magnetic moment. The other advantages of the rare-earth free Fe₃Sn system are its relatively low price and rather high T$_C$ of about 743 K [5]. However, as it has recently been shown both experimentally and theoretically,

---
[*]olga.vekilova@physics.uu.se

the magnetocrystalline anisotropy of Fe_3Sn is planar, which is undesirable for a permanent magnet [6]. It has also been suggested by Sales *et al.* that alloying with Sb might change the anisotropy to uniaxial [6]. Motivated by this research, we studied the influence of different dopants on the MAE of the Fe_3Sn compound. The electronic structure and magnetic properties, as well as the effect of the hexagonal c/a ratio on the magnetocrystalline anisotropy in the Fe_3Sn compound and its alloys, were addressed from first principles by means of highly accurate full-potential linear muffin-tin orbital (LMTO) method implemented in the RSPt code. The stability of the doped phases were elucidated by the calculation of formation enthalpies by means of the Vienna Ab initio Simulation Package (VASP).

Theoretical calculations were combined with an experimental study to verify the phase stability as well as the magnetic properties of Fe_3Sn compounds. Combinatorial materials science and high-throughput screening methods, such as reactive crucible melting (RCM) technique, offer an efficient strategy for the discovery of new materials with promising properties. Using the knowledge of the required synthesis conditions for the formation of the Fe_3Sn phase [7], we performed the RCM method to search for the $Fe_3(SnM)$ phase. To get more insight into the magnetic properties of the $Fe_3(SnM)$ phase, additional experiments were performed using the solid state reaction (SSR) method, which was used for the preparation of the desirable compound from the mixture of the starting elements by means of atomic diffusion. For the most promising system, a micromagnetic model was developed to calculate the magnetic induction as a function of the internal field.

The paper is organized as follows. Section II A describes theoretical methods used for the first-principles calculations. Section II B provides the experimental details. In Secs. III A, III B, III C, and III D, the results of theoretical simulations as well as experimental results are given. Section III E addresses the results of the micromagnetic simulations. Conclusions are given in Sec. IV.

II. METHODS

A. Theory

The high-temperature phase of Fe_3Sn has a hexagonal crystal structure with space group $P6_3/mmc$ (#194) and contains eight atoms per unit cell (see Fig. 1). For calculations of phase stability, VASP [8–10] was used within the projector augmented wave (PAW) method [11]. The electronic exchange and correlation effects were treated by the generalized gradient approximation in the Perdew, Burke, and Ernzerhof (PBE) form [12] in all used methods. A 64-atom supercell of Fe_3Sn comprising 46 Fe and 16 Sn atoms was considered. The plane-wave energy cutoff was set to 350 eV. The converged k-point mesh was found to be $8 \times 8 \times 8$ k-points. The obtained magnetic moment on iron was $\sim 2.4 \mu_B$ per atom, in agreement with previous studies [6].

The Sn atoms of the Fe_3Sn compound were partially replaced by alloying elements. To examine the phase stability of considered doped systems for each $M = $ Sb, Ga, Ge, and Hf, we calculated three different distributions of M atoms, namely ordered, random (i.e., mimicking a disordered alloy), and
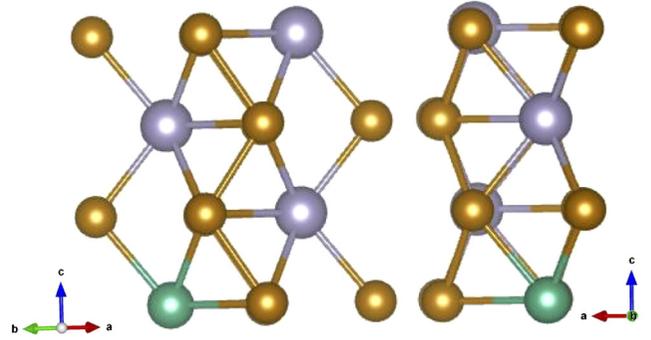

FIG. 1. $1 \times 1 \times 2$ hexagonal cell of Fe_3Sn with one dopant on the tin sublattice. Iron atoms are shown with brown spheres, Sn atoms with grey, and M ($M=$Si, P, Ga, Ge, As, In, Sb, Te, and Bi) dopant is shown with the green sphere.

phase separated (i.e., mimicking clusterization of dopants) (see Supplemental Material [13]). We used the special quasirandom structure (SQS) technique [14–16] to generate the corresponding supercells.

The $1 \times 1 \times 2$ supercell of Fe_3Sn comprising 12 iron and four tin atoms, one of which is further substituted by a dopant (see Fig. 1), was used for the calculation of the magnetic properties with help of the FP-LMTO method implemented in the RSPt code [17,18]. We performed integration over the Brillouin zone, using the tetrahedron method, with Blöchl's correction [19]. The k-point convergence of the MAE for the chosen supercell size was found when increasing the Monkhorst-Pack mesh [20] to $24 \times 24 \times 24$, which was further used in all calculations.

The following dopants were considered in $Fe_3Sn_{0.75}M_{0.25}$ compound: $M = $ Si, P, Ga, Ge, As, Se, In, Sb, Te, Pb, and Bi. With one substitutional M atom in the considered supercell, the dopant concentration is fixed to 6.25 at. %. The equilibrium lattice parameter and hexagonal c/a ratio were calculated for every structure using VASP. The effective exchange interaction parameters (J_{ij}) were obtained using the method of Lichtenstein *et al.* [21,22], as implemented in RSPt [23]. In this technique, the energy of the system is mapped onto a classical Heisenberg model with the following Hamiltonian:

$$\hat{H} = -\frac{1}{2}\sum_{i \neq j} J_{ij}\vec{e}_i \cdot \vec{e}_j, \tag{1}$$

where $\vec{e}_i$ denotes the unit vector along the magnetic moment at the site i. The exchange parameter between sites i and j is defined in the following way:

$$J_{ij} = \frac{T}{4}\sum_n \text{Tr}[\hat{\Delta}_i(i\omega_n)\hat{G}_{ij}^{\uparrow}(i\omega_n)\hat{\Delta}_j(i\omega_n)\hat{G}_{ij}^{\downarrow}(i\omega_n)], \tag{2}$$

where T is the temperature, Δ is the on-site exchange potential, G_{ij} is an intersite Green's function and $i\omega_n$ is the nth fermionic Matsubara frequency [23].

B. Experiment

Screening through a large variety of material compositions and possible temperature stability ranges using traditional

equilibrium alloy approach, which is a one-alloy-at-a-time practice, is a laborious task. Combinatorial materials science and high-throughput screening methods enable the synthesis of large number of samples at once and therefore speed up the discovery of the new materials. Furthermore, using high-throughput characterization methods, their properties can be efficiently determined. Several phase diagrams of material systems have been constructed using different combinatorial approaches [24,25], e.g., thin film deposition [26] and bulk high-throughput techniques, such as reactive diffusion method [27], and RCM [7,28–32].

The RCM method is first introduced in Ref. [31] as a tool to search for hard magnetic phases. The method is based on diffusion processes driven by the formation of concentration gradient between the crucible material and other elements which are filled into it. Production procedure and working principle of the RCM method is fully described in Ref. [7], where the method is applied to the Fe-Sn binary system and all five known intermetallic compounds of the system were synthesized in the reactive crucibles. The Fe_3Sn (3:1) phase was obtained in RCM by quenching of the crucibles after annealing at high temperatures (1023 K–1098 K).

To explore the hexagonal Fe_3Sn phase in the quest for uniaxial anisotropy, Fe-$Sn_x M_{1-x}$ crucibles with M = Sb, Si, Ga, Ge, Pb, In, Bi and $0.5 < x < 0.75$ were synthesized. To further extend our search, quaternary Fe-Mn, Sn, Sb crucibles were additionally produced. The crucibles were made of 99.95% pure Fe and they were filled with about 1 g of the rest elements of the examined system. The filling elements with the purity > 99.9 were added in the form of crushed pieces. The samples were annealed at three selected temperatures of 1013 K, 1043 K, and 1073 K for one week and subsequently quenched. The selected annealing temperatures were chosen in accordance with the Fe-Sn phase diagram from the temperature range where the binary Fe_3Sn phase is stable. For details, we refer to Ref. [7].

For high-throughput characterization, the microstructure of the formed phases was studied by Philips XL30 FEG scanning electron microscopy (SEM) in backscattered electron (BSE) contrast mode and their chemical compositions were determined using energy dispersive x-ray (EDX) spectroscopy. In addition, a Zeiss Axio Imager.D2m magneto-optical Kerr effect microscopy (MOKE) was used to display the magnetic domain structure of the formed phases, which may give a clear hint for identification of the phases with uniaxial anisotropy.

Several Fe$_y$Mn$_{3-y}$Sn$_x$Sb$_{1-x}$ samples ($y = 3$ and $x = 1$; $y = 2.5, 2.25, 2,$ and 1.5, and $x = 0.75$; and $y = 1.5$ and $x = 0.9$) were prepared by SSR [33] through the following procedure. First, stoichiometric amounts of powders of the starting elements (99.9+% purity, particles of less than 50 microns in size) were hand milled with an agate mortar and pestle and then compacted into pellets using pressures up to 0.5 GPa at room temperature. Pellets were then encapsulated in a quartz ampoule, heated to 1073 K for 48 h in vacuum and then quenched into ice water.

This process was repeated twice to homogenize the composition in the sample. X-ray diffraction (XRD) measurements were performed on a Philips X'Pert Pro diffractometer in the Bragg-Brentano geometry, using Cu Kα radiation (λ = 1.5418 Å). The samples were placed on a spinner to avoid
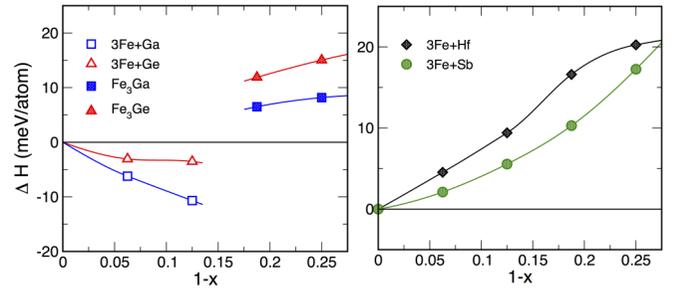

FIG. 2. Enthalpy of formation (ΔH) of the ternary $Fe_3Sn_x M_{1-x}$ [M = Ga, Ge (a) and Sb, Hf (b)] compound as a function of the concentration of dopant M, calculated in comparison with the Fe_3Sn binary on the left-hand side of both (a) and (b). On the right-hand side of (a) Fe_3M (M = Ga, Ge) binary compound, shown with filled symbols or a mixture of Fe and M = Ga, Ge, shown with open symbols, were used, while in (b) only the mixture of Fe and M = Sb and Hf element was used for the enthalpy comparison.

a possible preferential crystalline orientation. XRD patterns were analyzed by Rietveld refinements, through the FullProf Suite [34], using a Thompson-Cox-Hastings pseudo-Voigt function to describe the profile of the peaks. Temperature-dependent magnetization was measured up to 823 K, using $H = 0.01$ T, in a vibrating sample magnetometer EZ7-VSM from Microsense.

III. RESULTS

A. Phase stability

To estimate stability of a ternary compound, one needs to use as reference points the enthalpies of stable binary compounds at proper concentrations. In the case of Fe_3Sn-M, which is expected to be a high-temperature phase (similar to Fe_3Sn), we wanted to compare with the corresponding high-temperature 1:3 binary phases, provided they are stable. We took for comparison Fe_3Sn and Fe_3M, where it was possible. If there were no stable 1:3 phases, we compared with the mixture of pure elements. In this estimation, we avoided a comparison with the low-temperature phases, like FeSn and Fe_3Sn_2, as at conditions of our calculations (0 K) they would always be more stable.

To estimate phase stability of ternary compounds, when both corresponding binary phases are stable, the following equation was used:

$$\Delta H = H_{Fe_3Sn_x M_{1-x}} - x H_{Fe_3Sn} - (1 - x) H_{Fe_3M}, \quad (3)$$

where $H_{Fe_3Sn_x M_{1-x}}$ is the enthalpy of a ternary compound and x is the concentration of Sn. In the other case, when only one phase was stable, a comparison with the mixture of pure elements was used according to the following equation:

$$\Delta H = H_{Fe_3Sn_x M_{1-x}} - x H_{Fe_3Sn} - (1 - x)(3H_{Fe} + H_M), \quad (4)$$

where H_{Fe} and H_M are enthalpies of pure Fe and M-dopant, respectively.

The enthalpy of formation was calculated for ternary $Fe_3Sn_{0.75}M_{0.25}$ alloys, where M = Sb, Ga, Ge, and Hf for different concentrations of dopants from 6.25, 12.5, 18.75, and up to 25 at. % (see Fig. 2). A positive slope of the

enthalpy of formation at $x \to 0$ indicates an unstable ternary compound, while the negative one corresponds to a stable structure. The enthalpies of these systems were examined and compared with the energies of the binary Fe_3Sn compound on the left-hand side and binary Fe_3M [Eq. (3)] or the mixture of pure Fe and M (if the binary phase was not energetically favorable [Eq. (4)] on the right-hand side of Fig. 2.

Investigating the phase diagrams of the Fe-Ga and Fe-Ge binaries [35,36] one can see that in the region up to 10–20 at. % of dopant elements at temperatures up to 1500 K the Fe_3M phase decomposes into a mixture of α-Fe and pure Ga or Ge phases [35,36]. At higher concentration of dopants the phase is, however, stable. For this reason, enthalpy of $Fe_3Sn_{0.75}M_{0.25}$ (M = Ga, Ge) was calculated relative to both the mixture of pure elements as well as the Fe_3M (M = Ga, Ge) phase, see Fig. 2(a). The empty area around 15 at. % of dopant concentration corresponds to the region where both the mixture of elements and binary phases might exist, depending on temperature and the dopant.

At a concentration of dopants lower than ∼15 at. %, when compared to the mixture of pure elements on the right-hand side, the enthalpy is negative, indicating stability of the structure [see red and blue lines with open symbols in Fig. 2(a)]. However, when compared with the binary phase Fe_3M, the stability of the ternary structure should be estimated from the upper positive curves for both Ga and Ge dopants [see red and blue lines with filled symbols in Fig. 2(a)].

In the considered $Fe_3Sn_{0.75}M_{0.25}$ alloy, the concentration of dopants is equal to 6.25 at. %, which means the structures could be considered as stable, based on this theoretical estimation.

In contrast, checking the phase diagram of Fe-Sb one can see that the binary Fe_3Sb phase cannot exist. Furthermore, when the formation enthalpy of $Fe_3Sn_{0.75}Sb_{0.25}$ phase was calculated in comparison with the mixture of pure elements on the right-hand side [see the green curve in Fig. 2(b)] it appeared that the phase is unstable. However, as described in Sec. III B, this phase has promising magnetic properties. In Ref. [6], it was shown experimentally that doping with Mn on the Fe site stabilizes the $Fe_3Sn_xSb_{1-x}$ phase. Accordingly, Mn was added to the Fe sublattice of $Fe_3Sn_{0.75}Sb_{0.25}$ for further experimental observations and theoretical calculations of magnetic properties, see Secs. III B–III D.

Similarly, for the Hf dopant, even comparing with the mixture of elements [see the black line in Fig. 2(b)], the enthalpy curvature is positive indicating thermodynamic instability of this phase. For that reason, Hf was further excluded from consideration and calculation of the magnetic properties.

B. Magnetocrystalline anisotropy

We calculated the saturation magnetic moment of $Fe_3Sn_{0.75}M_{0.25}$ system. For the pristine Fe_3Sn it is equal to $\mu_0M_s = 1.49$ T, or $M_s = 1.19$ MA/m, in very good agreement with previous theoretical and experimental estimations [6]. Due to the low concentration of the dopants, 6.25 at. %, in the doped system, the obtained value of saturation magnetization is close to the one of the undoped system. For instance, for the case of Sb substitution it is equal to 1.51 T, or 1.2 MA/m.

III		IV		V		VI	
		Si	-0.62	P	-0.45		
Ga	-0.87	Ge	-0.36	As	0.23	Se	-0.22
In	-2.27	Sn	-1.50	Sb	0.33	Te	0.09
		Pb	-1.77	Bi	-0.06		

FIG. 3. Calculated values of magnetocrystalline anisotropy energy (MAE), K_1 (MJ/m^3), and easy magnetization direction for different dopants in Fe_3Sn alloy grouped according to the positions of dopants in the periodic table. A negative value of K_1 indicates the in-plane easy magnetization axis, while the positive one shown with the filled blue rectangulars corresponds to the desirable uniaxial magnetocrystalline anisotropy. The saturation magnetic moments in all the systems are similar and close to $\mu_0M_s = 1.5$ T.

Magnetocrystalline anisotropy of the $Fe_3Sn_{0.75}M_{0.25}$ system, where M = Si, P, Ga, Ge, As, Se, In, Sb, Te, Pb, and Bi was calculated from first-principles electronic structure theory. The resulting MAE values are shown in Fig. 3 for the dopants grouped according to their positions in the periodic table. For the pristine Fe_3Sn, the resulting anisotropy was found to be equal to -1.5 MJ/m^3 (see Fig. 3). In magnitude, this is one of the largest values among all the considered structures; however, the minus sign indicates the easy plane of magnetization. These results are in good agreement with other theoretical and experimental estimations (-1.59 MJ/m^3 and -1.8 MJ/m^3, respectively [6]).

As one can see in Fig. 3, the largest magnitude of the MAE (albeit favoring in-plane easy axis), of all the considered structures with dopants, was obtained for the $Fe_3Sn_{0.75}In_{0.25}$ compound. An uniaxial anisotropy was found for M = As, Sb, and Te. However, the MAE for the Te doping is very small. The anisotropy of $Fe_3Sn_{0.75}Sb_{0.25}$ is in agreement with the existing theoretical data of 0.5 MJ/m^3 [6].

The obtained MAE data of the $Fe_3Sn_{0.75}M_{0.25}$ system were plotted as a function of the number of valence electrons per formula unit for doping atoms from three rows of the periodic table, see Fig. 4. Positive numbers correspond to a uniaxial MAE. As one can see, a similar tendency is shown for the anisotropy in all considered rows. Starting from the lowest values, corresponding to high but planar anisotropy, for the dopants from the Group IIIA (Ga and In) the MAE moves towards positive values, with an increase of the number of valence electrons in the system. The maximal value of MAE, which is positive for As and Sb dopants, is obtained for Group VA elements. This tendency is shown for all the considered rows of elements, notifying that Group VA dopants seem to be the most promising for the consideration, specifically As and Sb. Two other elements of this group, P and Bi, do not flip anisotropy to uniaxial (see Fig. 3).
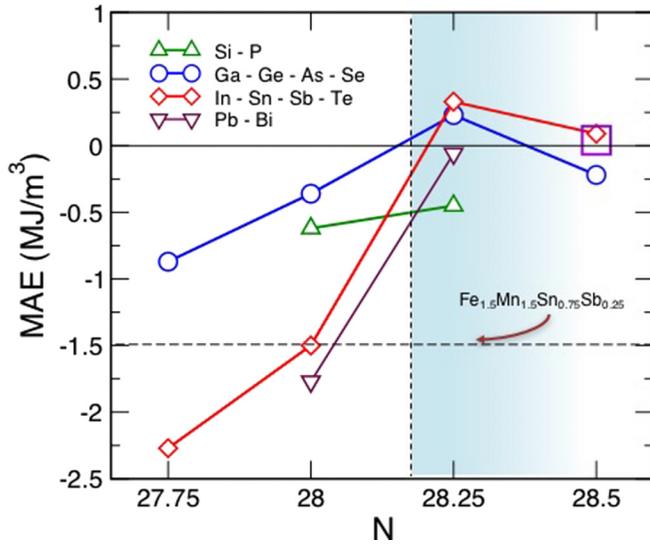
FIG. 4. The magnetocrystalline anisotropy energy (MAE) in $Fe_3Sn_{0.75}M_{0.25}$ compound as function of the number of valence electrons, N, of the system for four rows: Si-P (shown with the green triangles up), Ga-Ge-As-Se (shown with the red diamonds), In-Sn-Sb-Te (shown with the blue circles), and Pb-Bi (shown with the violet triangles down). Doping from Group IIIA, Group IVA, Group VA, and Group VIA, correspond to $N = 27.75$, 28.25, and 28.5, respectively. The area of interest, where the easy magnetization axis is uniaxial, is shown with the gradient background. The horizontal dashed line shows the magnitude of the $Mn_{1.5}Fe_{1.5}Sn_{0.75}Sb_{0.25}$ anisotropy, as its number of valence electrons is substantially lower. Large open square represents the anisotropy of $Fe_3Sn_{0.5}Sb_{0.5}$.

To illustrate the dependence of MAE on the number of valence electrons, the MAE for the case of increased Sb content, i.e., $Fe_3Sn_{0.5}Sb_{0.5}$, was calculated. In this system, the number of valence electrons is 28.5, the same as in the $Fe_3Sn_{0.75}Te_{0.25}$ system. Surprisingly, the MAE does not increase with the increase of the Sb content and the obtained value of 0.04 MJ/m^3 (shown with the large open square in Fig. 4) is barely positive and rather close to the value calculated for $Fe_3Sn_{0.75}Te_{0.25}$.

As mentioned in Sec. III A, to stabilize the $Fe_3Sn_{0.75}Sb_{0.25}$ system, Mn was added on the Fe sublattice (see Fig. 5). The addition of Mn changes anisotropy back to planar. The increase of Mn content leads to the increase of absolute value of anisotropy. The anisotropy of $Fe_{1.5}Mn_{1.5}Sn_{0.75}Sb_{0.25}$ system is equal to -1.49 MJ/m^3, which is very close to the value for the undoped Fe_3Sn system. It is also shown in Fig. 4 with the horizontal dashed line for comparison. The number of valence electrons in the unit cell of this system is 26.75, which is out of the scale of Fig. 4. Adding Sb to the pristine Fe_3Sn allows for the change of anisotropy from planar to uniaxial, while adding Mn for stabilization reverts it back to planar.

The dependence of the magnetic properties on the number of valence electrons in dopants was further considered by the calculation of the Heisenberg exchange parameters J_{ij}s between the iron atoms (see Fig. 6). The Fe_3Sn system, as well as all systems with dopants, were shown to be strongly ferromagnetic as indicated by large and positive J_0 (defined as a sum of all J_{ij}'s). Notice that the value of the nearest-neighbor
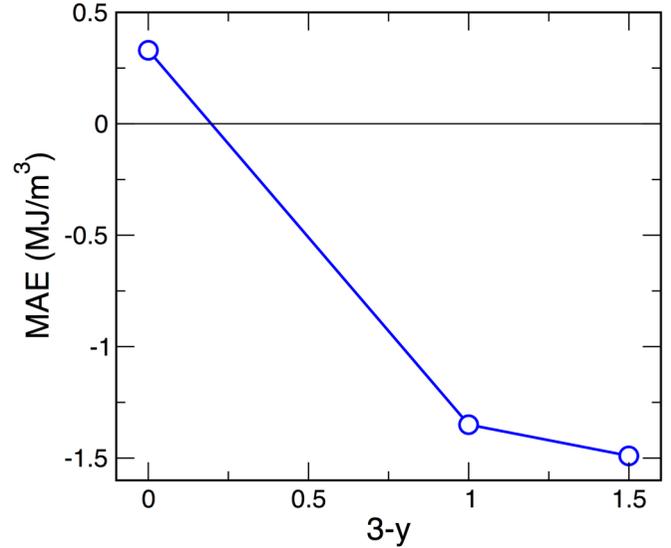

FIG. 5. The magnetocrystalline anisotropy energy (MAE) in $Fe_yMn_{3-y}Sn_{0.75}Sb_{0.25}$ compound as a function of the Mn content, 3-y, on the Fe sublattice of the system. The area below zero corresponds to the planar anisotropy while the area above zero represents the uniaxial anisotropy.

interaction, corresponding to the shortest interatomic distance, of $Fe_3Sn_{0.75}Sb_{0.25}$ system ($\sim$1.98 mRy) is slightly higher than that of Fe_3Sn ($\sim$1.75 mRy). Taking into account that the other interactions for these systems look rather similar, one can expect the increase of Curie temperature for the system with Sb dopant.

Taking into account that atomic relaxations substantially influence the MAE, we also studied the effect of the hexagonal lattice ratio, c/a, on the value of MAE. Figure 7 shows the change of the MAE when the c/a ratio increases from 1.4 to 1.9 for $Fe_3Sn_{0.75}M_{0.25}$ ($M = $ Sn, Ge, As and Sb) systems at a
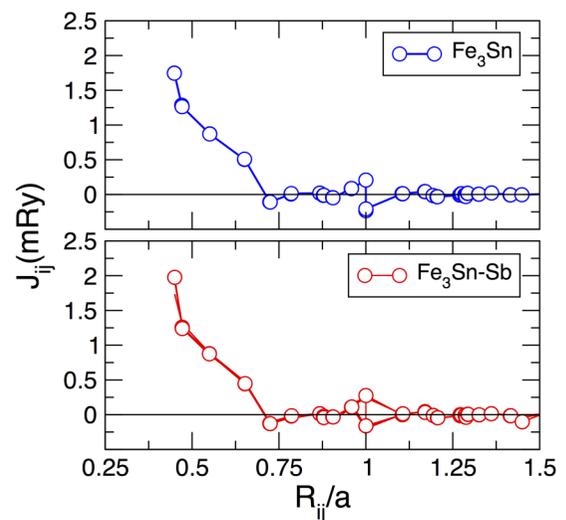

FIG. 6. Intersite exchange parameters J_{ij} between the iron atoms i and j separated by the distance R_{ij} of pristine Fe_3Sn compound (a), as well as of $Fe_3Sn_{0.75}Sb_{0.25}$ (b). System with planar MAE is shown with the blue lines, while system with uniaxial MAE is shown with red lines. a stands for the lattice constant.
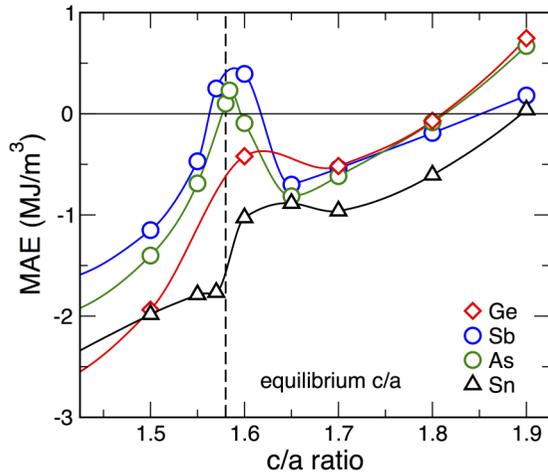
FIG. 7. Dependence of the magnetocrystalline anisotropy on the hexagonal c/a ratio for $M =$ Sn, Ge, As, and Sb dopants. The averaged equilibrium c/a ratio about 1.58 is shown with the dashed line.

fixed equilibrium volume. The averaged equilibrium c/a ratio ($\sim$1.58) is shown with the vertical dashed line. As the dopant concentration is low (6.25 at. %) the deviations from 1.58 of the c/a ratio for different dopants are rather minor.

For all considered dopants, the MAE behavior with the c/a increase is basically linear, illustrating that when the crystal is stretched, the easy axis can be switched from planar to uniaxial for all the structures. For instance, for Ge-doped Fe_3Sn a change of the c/a ratio at the fixed volume leads to the change of the anisotropy value from rather high with planar easy magnetization direction, $\sim-2.7\,\mathrm{MJ/m^3}$, to almost $\sim0.7\,\mathrm{MJ/m^3}$ with uniaxial easy magnetization direction. This strain induced change is largest for Ge doping, out of all considered dopants. It is worth noting that changing MAE to uniaxial requires a variation of c/a from $\sim$1.58 to 1.8, corresponding to 14%. In the experiment, it is hardly possible to change c/a of such systems by more than a few percent without structural changes, i.e., without altering the hexagonal structure.

It is important to mention that for all the structures there is a peak of the MAE vs c/a curve (Fig. 7) in the region near the equilibrium c/a. In some cases, like for $M =$ Sb and As, it can lead to the switching of the easy magnetization direction; however, this region is rather narrow and a small change in the c/a ratio (like 0.5% from the equilibrium) can switch the axis from planar to uniaxial and back. The highest peak is for Sb-doped Fe_3Sn; it corresponds to the highest anisotropy value and uniaxial easy magnetization direction.

For Ge-doped structure, as well as for the binary Fe_3Sn, slight modifications of the c/a near the equilibrium are not resulting in the MAE peak sufficiently high to switch the easy magnetization direction.

It is interesting to notice that for these two structures the peak is not exactly at the equilibrium c/a ratio but shifted, meaning that the small change of the c/a ratio due to, for instance, alloying or heating, can slightly increase anisotropy for some structures. Therefore, we underline that the MAE of Fe_3Sn with any of the dopants turns out to be very sensitive to the change of c/a.

C. Reactive crucible melting technique

The effect of substituting Sn by its neighboring elements was experimentally studied by high-throughput RCM method and the production of $Fe\text{-}Sn_x M_{1-x}$ crucibles, $M =$ Sb, Si, Ga, Ge, Pb, In, Bi and $0.5 < x < 0.75$. The diffusion zone of the crucibles annealed at the selected temperatures in the temperature interval from 1013 K to 1073 K were carefully screened by the EDX analysis. None of the substitutional elements could stabilize the 3:1 structure under the chosen conditions (for details on the results, see Supplemental Material [13]). It should be noted that although combinatorial approaches allow a rapid and efficient investigation of the phase evolution in intermetallic compounds, the accuracy and completeness of these methods are sometimes lower than in conventional metallurgical experiments, see Ref. [7]. An important issue is the so-called problem of missing phases, which refers to the fact that there may exist some phases that are present in the equilibrium alloy but they are not forming by interdiffusion reactions. For example, in Ref. [7] it was found that for the Fe-Sn system the RCM gives correct results in a wide temperature range except for the temperatures near 800 °C. The Fe_5Sn_3 phase, forming in conventionally melted alloys at 800 °C, does not exist in the diffusion zone of the reactive crucible annealed at the same temperature. The possible reasons for the observed discrepancies are given in Ref. [7].

Our theoretical calculations predict the change of anisotropy from planar to uniaxial in Fe_3Sn system by partial substitution of Sn by Sb. However, the formation enthalpy plot shows that $Fe\text{-}Sn_xSb_{1-x}$ is unstable in the addressed concentration range (see Fig. 2). Besides that, it was experimentally found that Sb destabilized the formation of 3:1 structure and instead the $Fe_3(Sn,Sb)_2$ phase was formed. This phase is not desirable for permanent magnet applications due to the small concentration of Fe and therefore low magnetization as well as its negligible MAE [6,7]. For stabilization of $Fe_3(Sn,Sb)$ phase, substitution of Fe by Mn (with one less electron) was suggested to be effective to compensate an extra electron of Sb in comparison to Sn. Accordingly, the $Fe\text{-}Mn_{0.75}Sn_{0.5}Sb_{0.5}$ and $Fe\text{-}Mn_{1.5}Sn_{0.75}Sb_{0.25}$ crucibles were synthesized and annealed in the temperature range of 1013 K to 1073 K.

It was found that Mn and Sb substitution preserved the hexagonal Ni_3Sn structure of the parent Fe_3Sn phase and $(Fe,Mn)_3(Sn,Sb)$ phase formed in the quaternary reactive crucibles. Figure 8 shows the microstructure forming in the diffusion zone of the $Fe\text{-}Mn_{0.75}Sn_{0.75}Sb_{0.25}$ reactive crucible annealed at 1073 K for five days and subsequently quenched. A thin layer of $(Fe_{0.6}Mn_{0.4})_3(Sn_{0.75}Sb_{0.25})$ phase is formed and bordered by Fe crucible. In addition, $(Fe_{0.5}Mn_{0.5})_3(Sn_{0.75}Sb_{0.25})_2$ phase is formed in large quantity on top of the 3:1 phase. The phase stability of the Sb-Mn doped Fe_3Sn compound is confirmed by RCM. However, to measure magnetic properties, such as M_s, T_C, and MAE; a single-phase material has to be synthesized. That was done by the SSR.

D. Solid state reaction

Several $Fe_y Mn_{3-y} Sn_x Sb_{1-x}$ samples ($y = 3$ and $x = 1$; $y = 2.25$, 2, 1.5, and $x = 0.75$; and $y = 1.5$, and $x = 0.9$) with different concentrations of Mn and Sb were prepared
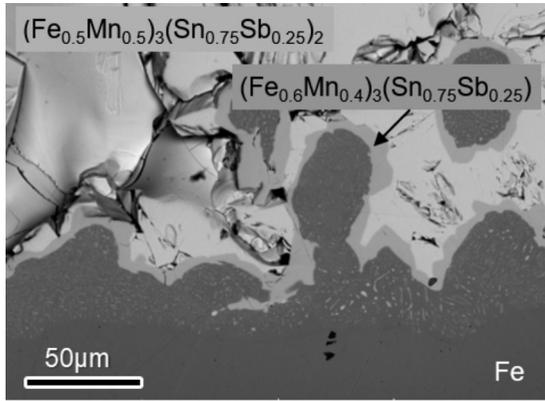
FIG. 8. BSE image of the $(Fe_yMn_{1-y})_3Sn_{0.75}Sb_{0.25}$ crucible annealed at 1013 K. Narrow layer of $(Fe_{0.6}Mn_{0.4})_3(Sn_{0.75}Sb_{0.25})$ is formed. However 3:2 phase is the dominant forming phase in the crucible.

by SSR. XRD patterns of the produced samples by two subsequent SSRs are shown in Fig. 9. For all the samples, the 3:1 phase was found though only for the parent Fe_3Sn alloy we found a single phase. Rietveld refinements were performed on all the XRD patterns and the results are shown in Table I.

The lattice parameters of the alloys (see Table I and Fig. 10) follow an increasing trend for higher values of the Mn concentration. The dependence of the lattice parameters on the concentration of Sb was not studied as only two points were available.

Temperature-dependent magnetization curves M(T) were measured for two selected samples with the highest amount of the 3:1 phase, namely Fe_3Sn, and with equal concentration of Fe and Mn, $Fe_{1.5}Mn_{1.5}Sn_{0.75}Sb_{0.25}$. The M(T) curves are shown in Fig. 11. The calculation of the Curie temperatures were performed by the derivative of the M(T). The obtained Curie temperature of Fe_3Sn system, $T_C = 748$ K, is rather high and in very good agreement with the existing experimental data ($T_C = 743$ K [5] and $T_C = 725$ K [6]), while that of the diluted sample, 393 K, is much lower than that of the parent composition Fe_3Sn. Similar values were found previously in
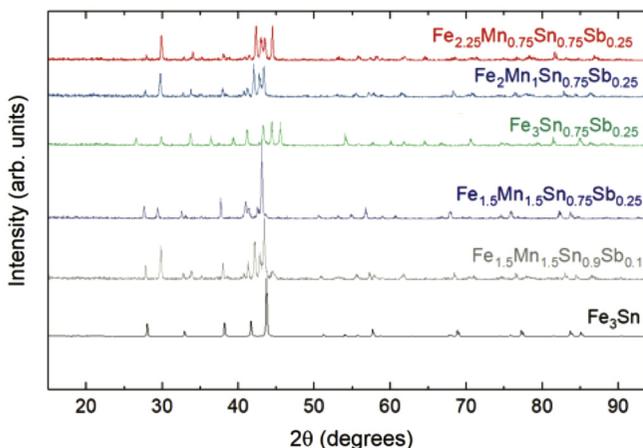
TABLE I. Lattice parameters of the $Fe_yMn_{3-y}Sn_xSb_{1-x}$ alloys, obtained by Rietveld refinements of the XRD patterns.

Sample	a(Å)	c(Å)
Fe_3Sn	5.4621(5)	4.3490(6)
$Fe_{2.25}Mn_{0.75}Sn_{0.75}Sb_{0.25}$	5.4858(5)	4.3721(6)
$Fe_2Mn_1Sn_{0.75}Sb_{0.25}$	5.5000(4)	4.3829(6)
$Fe_{1.5}Mn_{1.5}Sn_{0.75}Sb_{0.25}$	5.5338(1)	4.4270(2)
$Fe_{1.5}Mn_{1.5}Sn_{0.9}Sb_{0.1}$	5.5545(3)	4.4453(4)

literature for $Fe_{1.5}Mn_{1.5}Sn_{0.9}Sb_{0.1}$ and $Fe_{1.5}Mn_{1.5}Sn_{0.85}Sb_{0.15}$, with $T_C = 405$ K [6].

To examine how the addition of Mn to the $Fe_3(SnSb)$ compound affects the anisotropy, the domain structure of the formed 3:1 phase was investigated. For the ferromagnets with uniaxial anisotropy observation of characteristic domain patterns, namely stripe or branched domains, is expected. However, our Kerr analysis on the formed Mn/Sb substituted 3:1 phase shows nonuniaxial domain structure. This observation agrees with the negative theoretical value of anisotropy for the $Fe_{1.5}Mn_{1.5}Sn_{0.75}Sb_{0.25}$ system.

E. Micromagnetic simulations

A micromagnetic model was developed to estimate the energy density product $(BH)_{max}$ and coercive field $\mu_0 H_c$ of a potential magnet made of $Fe_3Sn_{0.75}Sb_{0.25}$. Using the software tool Neper [37], we created a synthetic microstructure based on Voronoi tessellation as shown in Fig. 12.

The granular grain structure consisted of 27 grains with an average grain diameter of 50 nm. Each grain's spontaneous magnetization, anisotropy energy density were taken from *ab initio* calculations ($\mu_0 M_{s,grain} = 1.52$ T, $K_{u,grain} = 0.33$ MJ/m^3). The exchange stiffness constant was assumed to be $A_{ex,grain} = 10$ pJ/m. The grain's easy axes were randomized within a cone angle of 5 with respect to positive z axis.
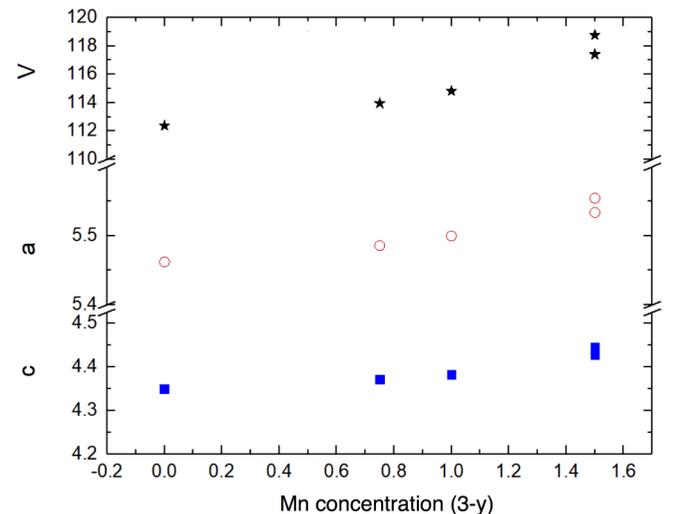

FIG. 9. XRD patterns of the $Fe_yMn_{3-y}Sn_xSb_{1-x}$ samples.

FIG. 10. Evolution of the lattice parameters and volume, obtained by Rietveld refinements of the XRD patterns, of the $Fe_yMn_{3-y}Sn_xSb_{1-x}$ alloys. These values are also shown in Table 1.
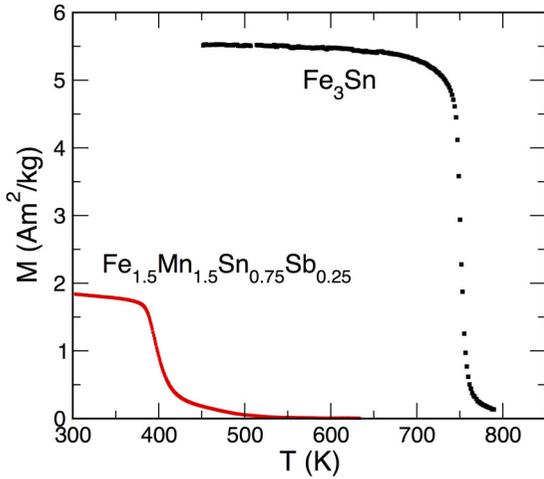
FIG. 11. M(T) curves for selected compositions within the $Fe_yMn_{3-y}Sn_xSb_{1-x}$ alloys. The abrupt drop corresponds to the Curie temperature, determined precisely by the derivative of the curve.

Between the grains, we assumed a 4-nm thick iron-rich ferromagnetic grain boundary phase ($K_{u,gb} = 0$). Its spontaneous magnetization was assumed to be $M_{s,gb} = 0.81$ T. Accordingly, the exchange stiffness constant was reduced to $A_{ex,gb} = 3.7$ pJ/m.

The magnetization value of the grain boundary phase was obtained by numerical optimization. We used the numerical optimization framework Dakota [38] and maximized the energy density product using $\mu_0 M_{s,gb}$ as a free parameter. The volume fraction of the grain boundary phase was 10%. The model was discretized into a uniform mesh with an edge length of 2 nm. A finite element energy minimization code [39] was used to compute the static hysteresis properties of the proposed model.

To compute the demagnetization curve, we calculated the equilibrium states for a subsequently decreasing external field H_{ext}. The field step $\mu_0 \Delta H_{ext} = -1$ mT. To compute the $B(H)$ loop and the expected energy density product, we corrected the loop which was obtained for a magnet with cubic shape with the macroscopic demagnetization factor $N = 1/3$.
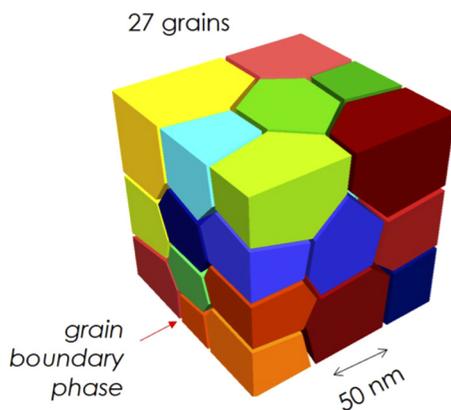

FIG. 12. Synthetic microstructure used for the simulation of the demagnetization curve of a nanocrystalline $Fe_3Sn_{0.75}Sb_{0.25}$ magnet.

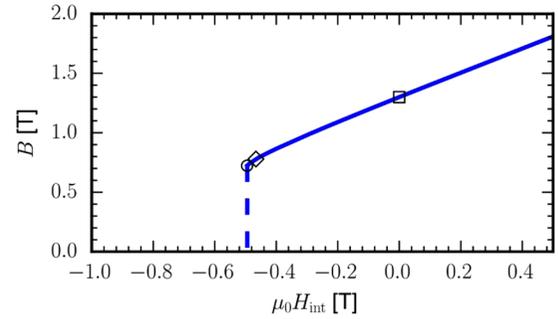FIG. 13. Computed $B(H)$ curve (magnetic induction as function of the internal field) for $Fe_3Sn_{0.75}Sb_{0.25}$. Remanence, energy density product, and coercive field are marked with a rectangle, diamond, and circle, respectively.

Figure 13 shows the computed $B(H)$ curve and Fig. 14 illustrates the equilibrium magnetic states before and after the first switching event, respectively. The computed coercive field is $\mu_0 H_c = -0.49$ T and the computed energy density product is 290 kJ/m^3. This is about 3/4 of the maximum energy density product reported for commercially available Nd-Fe-B magnets [2,40,41].

IV. DISCUSSION AND CONCLUSIONS

Electronic structure and magnetic properties of the hexagonal Fe_3Sn compound doped with 6.25 at. % of Si, P, Ga, Ge, As, Se, In, Sb, Te, Pb, and Bi were studied theoretically from first principles and experimentally. Our calculations show that at low concentrations of some dopants, such as Ga and Ge, the considered phases are stable. In contrast to that, in the case of the Sb dopant, the phase was shown to be unstable against decomposition into the mixture of pure elements. Our experimental study using RCM method supports this theoretical prediction that the addition of Sb into Fe-Sn system destabilizes the formation 3:1; however, further doping of Mn into the Fe sublattice stabilizes the structure. The SSR technique confirmed stabilization of the 3:1 phases with different concentrations of Mn.

Theoretical simulations predict that doping with As, Sb, and Te can change the easy magnetization direction to uniaxial. However, the change of the c/a ratio also substantially influences the MAE. In the case of Sb and As, the peak
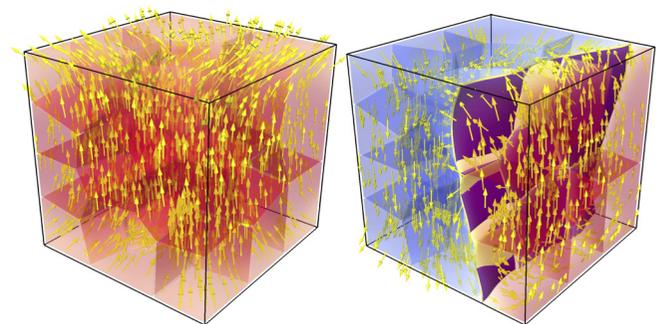

FIG. 14. During magnetization reversal domain walls become pinned near the grain boundaries.

in the MAE vs c/a dependence leads to the change of the easy magnetization axis from planar to uniaxial in the region close to the equilibrium c/a. For the Sb and As dopants, the region where anisotropy is uniaxial is rather narrow and even a small change of c/a, for instance, due to alloying with small amounts of Mn, can lead to the switch of the easy magnetization direction.

As follows from our calculations, the change of anisotropy due to addition of Mn to $Fe_3Sn_{0.75}Sb_{0.25}$ system turns uniaxial anisotropy back to planar. This estimation indicates that the predicted uniaxial anisotropy can hardly be observed experimentally. On one side, the presence of Mn stabilizes the Sb-doped alloy, but on the other side it basically flips the anisotropy back to the planar value of an undoped system. The experimentally stabilized $(FeMn)_3SnSb$ phase shows nonuniaxial domain structure in nice agreement with the theoretical prediction.

We studied all the dopants around Sn in the periodic table that can occupy the Sn sublattice and can likely be mixed with Fe_3Sn. From the MAE data grouped in the way as these dopants are placed in the periodic table of elements, one can see the tendency to increase the value of MAE from the III to the V group with the increase of the number of valence electrons. However, in the VI group there is a slight decrease for Te and Se, respectively. Thus, Group V seems to be the most promising out of all the considered groups and the Sb addition gives the largest uniaxial anisotropy. Looking at the vertical distribution in the periodic table, it appears that MAE increases from P to As and to Sb, but then for Bi there is a clear drop. Anisotropy depends more on the number of valence electrons than on the choice of a particular dopant. The MAE of the system doped with the most promising candidate, Sb, but with an increased amount of it as in $Fe_3Sn_{0.5}Sb_{0.5}$, is lower than that of $Fe_3Sn_{0.75}Sb_{0.25}$ and close to the value of the MAE in $Fe_3Sn_{0.75}Te_{0.25}$, i.e., the system with the same number of valence electrons. We conclude that the most preferable choice of dopants should be the column of the Group V elements in the periodic table, i.e., the one with As and Sb. Certainly, there is still a possibility

that other dopants can improve the desired properties of the Fe_3Sn if the proper number of valence electrons, close to the one in $Fe_3Sn_{0.75}Sb_{0.25}$, is created.

Further, the micromagnetic simulations allowed us to estimate the magnetic induction of the most promising system, $Fe_3Sn_{0.75}Sb_{0.25}$, as a function of the internal field. The computed coercive field is equal to -0.49 T. The calculated density energy product, 290 kJ/m^3, is at the level of best known to date magnets.

We investigated the $Fe_3Sn_{0.75}M_{0.25}$ system by different theoretical approaches as well as experimentally, to get a wider view on the magnetic properties of the system. Certain dopants, like Sb, can turn MAE of the hexagonal Fe_3Sn uniaxial. Furthermore, other magnetic properties of this system, such as saturation magnetization of 1.51 T and energy density product compatible with the values of the best known magnets are impressively high. However, such a turn of MAE is very sensitive to lattice deformations and the value of the magnetocrystalline anisotropy is reduced compared to the one of the parent phase. Further, the hexagonal phase becomes unstable with respect to decomposition. Addition of Mn allowed us to stabilize the system with dopants experimentally; however, the anisotropy turned back to planar. Therefore, further search for better stabilizers or their combinations (the so-called co-doping) might be considered to find the compromise between the stability and uniaxial MAE.

ACKNOWLEDGMENTS

[1] R. McCallum, L. Lewis, R. Skomski, M. Kramer, and I. Anderson, Annu. Rev. Mater. Res. **44**, 451 (2014).

[2] O. Gutfleisch, M. A. Willard, E. Brück, C. H. Chen, S. G. Sankar, and J. P. Liu, Adv. Mater. **23**, 821 (2011).

[3] M. D. Kuz'min, K. P. Skokov, H. Jian, I. Radulov, and O. Gutfleisch, J. Phys.: Condens. Matter **26**, 064205 (2014).

[4] K. Skokov and O. Gutfleisch, Scr. Mater. **154**, 289 (2018).

[5] G. Trumpy, E. Both, C. Djéga-Mariadassou, and P. Lecocq, Phys. Rev. B **2**, 3477 (1970).

[6] B. C. Sales, B. Saparov, M. A. McGuire, D. J. Singh, and D. S. Parker, Sci. Rep. **4**, 7024 (2014).

[7] B. Fayyazi, K. P. Skokov, T. Faske, D. Y. Karpenkov, W. Donner, and O. Gutfleisch, Acta Mater. **141**, 434 (2017).

[8] G. Kresse and J. Hafner, Phys. Rev. B **48**, 13115 (1993).

[9] G. Kresse and J. Furthmüller, Phys. Rev. B **54**, 11169 (1996).

[10] G. Kresse and J. Furthmüller, Comput. Mater. Sci. **6**, 15 (1996).

[11] P. E. Blöchl, Phys. Rev. B **50**, 17953 (1994).

[12] J. P. Perdew, K. Burke, and M. Ernzerhof, Phys. Rev. Lett. **77**, 3865 (1996).

[13] See Supplemental Material at http://link.aps.org/supplemental/10.1103/PhysRevB.99.024421 for the details of calculations of densities of states and RCM measurements, as well as for the comparison of different atomic distributions of dopants.

[14] A. Zunger, S.-H. Wei, L. G. Ferreira, and J. E. Bernard, Phys. Rev. Lett. **65**, 353 (1990).

[15] I. A. Abrikosov, S. I. Simak, B. Johansson, A. V. Ruban, and H. L. Skriver, Phys. Rev. B **56**, 9319 (1997).

[16] A. V. Ruban, S. I. Simak, S. Shallcross, and H. L. Skriver, Phys. Rev. B **67**, 214302 (2003).

[17] J. M. Wills and B. R. Cooper, Phys. Rev. B **36**, 3809 (1987).

[18] J. M. Wills, M. Alouani, P. Andersson, A. Delin, O. Eriksson, and O. Grechnyev, *Full-Potential Electronic Structure Method*, Springer Series in Solid State Science (Springer, Berlin, Germany, 2010), Vol. 167.

[19] P. E. Blöchl, O. Jepsen, and O. K. Andersen, Phys. Rev. B **49**, 16223 (1994).

[20] H. J. Monkhorst and J. D. Pack, Phys. Rev. B **13**, 5188 (1976).

[21] M. I. Katsnelson and A. I. Lichtenstein, Phys. Rev. B **61**, 8906 (2000).

[22] A. Liechtenstein, M. Katsnelson, V. Antropov, and V. Gubanov, J. Magn. Magn. Mater. **67**, 65 (1987).

[23] Y. O. Kvashnin, O. Grånäs, I. Di Marco, M. I. Katsnelson, A. I. Lichtenstein, and O. Eriksson, Phys. Rev. B **91**, 125133 (2015).

[24] K. Rajan, Annu. Rev. Mater. Res. **38**, 299 (2008).

[25] W. Maier, K. Stöwe, and S. Sieg, Angew. Chem. Int. Ed. **46**, 6016 (2007).

[26] K. Kennedy, T. Stefansky, G. Davy, V. F. Zackay, and E. R. Parker, J. Appl. Phys. **36**, 3808 (1965).

[27] J.-C. Zhao, J. Mater. Res. **16**, 1565 (2001).

[28] D. Goll, R. Loeffler, J. Herbst, R. Karimi, U. Pflanz, R. Stein, and G. Schneider, IEEE Trans. Magn. **50**, 1 (2014).

[29] D. Goll, R. Loeffler, J. Herbst, C. Frey, S. Goeb, T. Grubesa, D. Hohs, A. Kopp, U. Pflanz, R. Stein, and G. Schneider, Phys. Status Solidi RRL **9**, 603 (2015).

[30] S. Ener, J. Kroder, K. P. Skokov, and O. Gutfleisch, J. Alloys Compd. **683**, 198 (2016).

[31] A. Lüdtke, B. Stahl, I. R. Harris, and G. S. Schneider, *Proceedings of the 16th International Workshop on Rare-Earth Magnets and Their Applications* (Japan Institute of Metals, Sendai, 2000).

[32] F. Gross, Search for new permanent magnetic phases by reaction crucible analysis and development of high throughput methods, Ph.D. thesis, University of Birmingham, 2004.

[33] E. A. M. Lesley E. Smart, *Solid Sate Chemistry: An Introduction*, 3rd ed. (Taylor and Francis, Boca Raton, 2005).

[34] J. Rodríguez-Carvajal, Phys. B: Condens. Matter **192**, 55 (1993).

[35] B. Predel, Fe-Ga (iron-gallium), in *Dy-Er... Fr-Mo*, edited by O. Madelung (Springer, Berlin, 1995) pp. 1–4.

[36] B. Predel, Fe-Ge (iron-germanium), in *Dy-Er... Fr-Mo*, edited by O. Madelung (Springer Berlin, 1995) pp. 1–5.

[37] R. Quey, P. Dawson, and F. Barbe, Comput. Methods Appl. Mech. Eng. **200**, 1729 (2011).

[38] B. M. Adams, W. Bohnhoff, K. Dalbey, J. Eddy, M. Eldred, D. Gay, K. Haskell, P. D. Hough, and L. Swiler, DAKOTA, a multilevel parallel object-oriented framework for design optimization, parameter estimation, uncertainty quantification, and sensitivity analysis: version 5.0 users manual, Sandia National Laboratories, Tech. Rep. SAND2010-2183 (2009).

[39] J. Fischbacher, A. Kovacs, H. Oezelt, T. Schrefl, L. Exl, J. Fidler, D. Suess, N. Sakuma, M. Yano, A. Kato *et al.*, AIP Adv. **7**, 045310 (2017).

[40] S. Bance, F. Bittner, T. G. Woodcock, L. Schultz, and T. Schrefl, arXiv:1703.10710 [cond-mat.mtrl-sci].

[41] J. M. D. Coey, Scr. Mater. **67**, 524 (2012).